Environmental Science
Processes & Impacts

Accepted Manuscript

ROYAL SOCIETY OF CHEMISTRY

rsc.li/process-impacts

Table of contents entry:

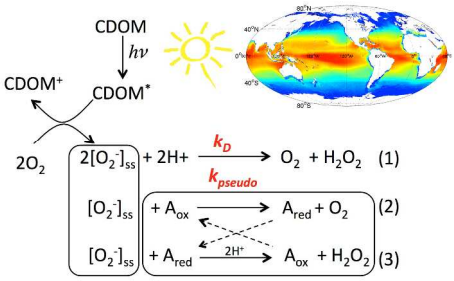

A novel combination of remote sensing products is used to estimate photochemical production rates of hydrogen peroxide and superoxide in the global surface ocean.

Environmental Impact Statement

A novel method for estimating photochemical production rates in the open ocean using remote sensing data is presented for hydrogen peroxide and superoxide. This approach provides quantitative information on these two reactive oxygen species, which is fundamental to fully understanding their role in changing redox chemistry in surface seawater.

Blending remote sensing data products to estimate photochemical production of hydrogen peroxide and superoxide in the surface ocean.

Leanne C. Powers[1] and William L. Miller[1*]
Department of Marine Sciences, University of Georgia, Athens, GA 30602, USA
*Corresponding author: bmiller@uga.edu

Hydrogen peroxide (H_2O_2) and its precursor, superoxide (O_2^-), are well-studied photochemical products that are pivotal in regulating redox transformations of trace metals and organic matter in the surface ocean. In attempts to understand the magnitude of both H_2O_2 and O_2^- photoproduction on a global scale, we implemented a model to calculate photochemical fluxes of these products from remotely sensed ocean color and modeled solar irradiances. We generated monthly climatologies for open ocean H_2O_2 photoproduction rates using an average apparent quantum yield (AQY) spectrum determined from laboratory irradiations of oligotrophic water collected in the Gulf of Alaska. Because the formation of H_2O_2 depends on secondary thermal reactions involving O_2^-, we also implemented a temperature correction for the H_2O_2 AQY using remotely sensed sea surface temperature and an Arrhenius relationship for H_2O_2 photoproduction. Daily photoproduction rates of H_2O_2 ranged from <1 to over 100 nM d^{-1}, amounting to ~30 μM yr^{-1} in highly productive regions. When production rates were calculated without the temperature correction, maximum daily rates were underestimated by 15 – 25%, highlighting the importance of including the temperature modification for H_2O_2 in these models. By making assumptions about the relationship between H_2O_2 and O_2^- photoproduction rates and O_2^- decay kinetics, we present a method for calculating midday O_2^- steady-state concentrations ($[O_2^-]_{ss}$) in the open ocean. Estimated $[O_2^-]_{ss}$ ranged from 0.1 – 5 nM assuming biomolecular dismutation was the only sink for O_2^-, but were reduced to 0.1 – 290 pM when catalytic pathways were included. While the

approach presented here provides the first global scale estimates of marine $[O_2^-]_{ss}$ from remote sensing, the potential of this model to quantify O_2^- photoproduction rates and $[O_2^-]_{ss}$ will not be fully realized until the mechanisms controlling O_2^- photoproduction and decay are better understood.

1. INTRODUCTION AND BACKGROUND

In the marine environment, photochemical reactions in surface waters lead to a number of oxidized products. The absorption of solar radiation by the chromophoric fraction of dissolved organic matter (CDOM) initiates reactions with molecular oxygen that lead to the formation of an array of reactive oxygen species (ROS), including superoxide (O_2^-), hydroxyl radical (OH•), singlet oxygen (O_2^1), and hydrogen peroxide (H_2O_2) (review by Burns et al.[1]). Of these, O_2^- is especially interesting in that it acts as both an oxidant and a reductant, as well serving as the precursor for H_2O_2, the longest lived ROS in the photic zone (Kieber et al.[2], references therein). Together, O_2^- and H_2O_2 (and OH• derived from them) are involved in degradation of organic pollutants and indirect photobleaching of CDOM,[3-5] creation of exogenous oxidative stress in aquatic organisms,[2,6-9] and alteration of redox cycling of trace metals like Fe, Cu and Mn.[2,10-13] Consequently, quantitative information on the production, sinks, and concentrations of O_2^- and H_2O_2 in the open ocean is fundamental to fully understanding their role in global biogeochemical cycles.

The formation of these reactive species in surface seawater begins with the absorbance of ultraviolet radiation (UVR; 280-400 nm) that elevates ground state CDOM to an excited state (CDOM*). Zhang et al.[14] suggest that CDOM* most likely generates

reactive intermediates via intramolecular charge transfer that subsequently reduce molecular oxygen to superoxide (O_2^- or its conjugate acid HO_2). O_2^- then decays through disproportionation to produce H_2O_2 via the following reactions:[15]

$$HO_2 + O_2^- \rightarrow HO_2^- + O_2 + OH^- \qquad (k_1 = 9.7 \times 10^7\ M^{-1}s^{-1}) \qquad (1)$$

$$HO_2 + HO_2 \rightarrow H_2O_2 + O_2 \qquad (k_2 = 8.3 \times 10^5\ M^{-1}s^{-1}) \qquad (2)$$

$$H^+ + O_2^- \longleftrightarrow HO_2 \qquad (K_a = 1.6 \times 10^{-5}\ M^{-1}) \qquad (3)$$

where k_1 and k_2 are rate constants determined in pure water at 25°C and K_a is the superoxide acidity constant.[16] Zafiriou[17] reported similar superoxide dismutation kinetics in seawater, determining a pKa of 4.60 ± 0.15, defining the overall second order rate law for O_2^- decay by dismutation as

$$\frac{d[O_2^-]}{dt} = k_{dis}[O_2^-][HO_2] \approx 2k_D[O_2^-]^2 \qquad (4)$$

where k_D for seawater = (5 ± 1) x $10^{12}[H^+]$, confirming a direct dependence on pH for O_2^- kinetics that has been verified by subsequent work.[18]

Laboratory studies have shown that UV-B radiation (280 to 320 nm) is the most efficient spectral region for production of H_2O_2 in marine systems, reflected in global distributions of H_2O_2 photoproduction rates.[15,19-21] These rates typically decrease with increasing latitude, in part due to decreasing UVR flux but also due to temperature differences between polar and equatorial waters. Because the rate limiting step for the photochemical formation of H_2O_2 is a thermal process (Equations 1, 2 and 4), the efficiency for H_2O_2 photoproduction typically increases by a factor of 2 for every 10°C increase in water temperature.[19] Szymczak and Waite[22] demonstrated that total H_2O_2 production under full spectral solar irradiation follows an Arrhenius rate law and calculated an activation energy (E_a) for the reaction of 37.4 kJ mol^{-1}. Instead of

74 determining an E_a from full spectrum irradiations, Miller[23] demonstrated that wavelength-
75 dependent activation energies could also be calculated from Arrhenius plots for H_2O_2
76 photoproduction. This data can therefore be used to quantify the change in H_2O_2
77 production efficiency due to temperature.

78 Comparing work done on H_2O_2 and O_2^-, H_2O_2 photoproduction has been studied
79 most extensively, not only due to its biogeochemical reactivity, but also due to its greater
80 concentration and stability relative to other ROS.[15] Additionally, the instability of O_2^- in
81 aqueous solutions makes analytical standards difficult to maintain, even when metal
82 chelators are added and alkaline pH is used to slow O_2^- loss rates.[24] Consequently, there
83 are currently no spectral photochemical efficiency data for the formation of O_2^- in surface
84 ocean waters, but as the primary photochemical precursor for H_2O_2 formation in sunlit
85 waters, it should be possible to infer O_2^- chemistry from H_2O_2 data.

86 Superoxide, and in turn H_2O_2 photoproduction rates, are controlled by the rate of
87 photon absorption ($Q_a(\lambda,z)$; mol(photons) m^{-3} s^{-1}) at a given wavelength (λ; m) and depth
88 (z; m) together with the efficiency of the reaction sequence; in other words, the
89 probability that absorption of solar radiation will lead to O_2^- or H_2O_2 formation. $Q_a(\lambda,z)$
90 is a function of CDOM "concentration" (defined with a spectral absorption coefficient,
91 $a_{g\,;}m^{-1}$), the solar spectral scalar irradiance ($E_0(\lambda,0^-)$; mol (photons) m^{-2} s^{-1} nm^{-1}), and its
92 attenuation in the water column ($K_d(\lambda)$; m^{-1}). This is quantified as

93 $$Q_a(\lambda,z) = E_0(\lambda,0^-)e^{-K_d(\lambda)z}a_g(\lambda,z) \quad (5)$$

94 For marine systems, the reaction efficiency is typically quantified spectrally as the
95 apparent quantum yield (AQY; $\varphi(\lambda)$), defined as the ratio of the number of moles product
96 produced to the number of moles of photons absorbed by CDOM in the sample.

Once $Q_a(\lambda,z)$ is defined, and assuming active photochemical production is confined to the 290 – 490nm wavelength range, *in situ* photochemical H_2O_2 production rates (P_{H2O2}; mol(H_2O_2) m^{-3} s^{-1}) in sunlit waters can be modeled as follows,

$$P_{H_2O_2} = \int_{290}^{490} Q_a(\lambda,z)\phi(\lambda,z)d\lambda \quad (6)$$

This general approach is appropriate for any scale for which the optical and photochemical variables can be defined and has been used to describe results ranging from laboratory irradiations in quartz containers[25] to global ocean calculations[26] from satellite data. This later development is critical for new examination of the importance of photochemical reactions over large spatio-temporal scales.

It is well known that the oceans are exhibiting increased temperatures,[27] salinity changes,[28] reductions in pH and changes in the calcium carbonate saturation point.[29] All of these affect marine redox kinetics. In order to assess the effects of widespread oceanic shifts on O_2^- and H_2O_2 cycling, we have employed the methods of Fichot and Miller[26] to examine the photochemical formation of these ROS from satellite data on a global scale. To define the variables discussed above ($E_d(\lambda,z)$, $K_d(\lambda)$, $a_g(\lambda,z)$ and $\varphi(\lambda,z)$), this study combines remotely sensed ocean color and sea surface temperature data with modeled solar irradiances and laboratory derived H_2O_2 AQY spectra corrected for temperature to calculate global H_2O_2 production rates in the surface ocean. New data for O_2^- kinetics from open ocean samples are then used to infer superoxide dynamics underlying the H_2O_2 photoproduction rates, providing insight into the global trends in the turnover rates of these two reactive oxygen species in a warmer and more acidic future ocean.

2. METHODS

2.1 Sample Treatment

Surface seawater samples, taken within the top meter, used for photochemical experiments in this study were collected from two locations: the Northern Gulf of Mexico onboard the R/V *Pelican* in May 2012 and in the Gulf of Alaska onboard the R/V *Melville* in August 2013. Samples were 0.2 μm gravity-filtered (Whatman; Polycap-36&75AS) directly from standard Niskin bottles into 1 L acid-cleaned (2 M HCl), ashed borosilicate glass bottles (Kimax; Gulf of Mexico) or 2 L acid-cleaned, Milli-Q (Millipore, >18 MΩ) rinsed polycarbonate bottles (Nalgene; Gulf of Alaska). Sample locations and properties relevant for photochemistry are listed in Table 1. Samples for H_2O_2 quantum yield determinations used in this study were stored at 4 °C in the dark for up to 3 months prior to use. CDOM absorption spectra are reported to exhibit no significant changes when stored in this manner for up to 12 months[30,31] and photochemical properties were assumed unchanged. Gulf of Alaska samples for shipboard superoxide irradiations were typically partitioned directly into acid-cleaned, Milli-Q rinsed, 600 mL jacketed beakers (Ace Glass) maintained at 20 °C with a recirculating water bath for photochemical experiments, either within hours of collection or stored on the ship at 4 °C until use, typically 1-2 days. While all equipment in contact with seawater samples was acid-cleaned as described above and gloves were used in handling samples, neither the *RV Pelican* nor the *RV Melville* was equipped with special trace metal processing facilities and consequently, limited trace metal contamination could be present.

2.2 Optical Measurements

Three separate systems were employed for solution absorbance measurements. A Perkin Elmer Lamda 40 dual beam spectrophotometer was used for H_2O_2 standard determinations and CDOM samples. For superoxide standard determinations, an Ocean Optics Inc. system composed of a DT-MINI-2-GS light source linked to a USB2000-UV-VIS Miniature Fiber Optic Spectrometer with Premium grade Si fiber optic assemblies allowed real-time absorbance measurements in a 1 cm cell. For oligotrophic seawater used in H_2O_2 AQY calculations and superoxide irradiations, the USB2000 was replaced with a MAYA2000-Pro UV-VIS spectrometer (Ocean Optics) and connected to a LWCC-2100 Type II, 1-meter liquid waveguide capillary flow cell (World Precision Instruments) to check CDOM measurements on the same samples made using the Lambda 40. The LWCC was filled via a peristaltic pump positioned to pull from glass sample bottles through Teflon tubing. CDOM and H_2O_2 baselines were zeroed against Milli-Q water and pre-irradiated acetone/ethanol for superoxide standards as described below.

2.3 Laboratory Determinations of ROS

2.3.1 ***Hydrogen Peroxide Analysis:*** H_2O_2 was measured using a FeLume chemiluminescence (CL) system (Waterville Analytical) and modifications to the methods of King et al.[32] Briefly, H_2O_2 in samples will chemiluminesce at alkaline pH when mixed in a flow injection analytical system with 2 μM 10-methyl-0-(*p*-formylphenyl)-acridinium carboxylate trifluoromethanesulfonate (AE; provided by Dr. James J. Kiddle, Western Michigan University). A syringe was used to flush (≥1 mL)

and fill a 195 µL Teflon sample loop (VICI 10-port valve) that was subsequently moved with carrier to mix with the AE reagent and then transported to a spiral flow cell located in front of a photomultiplier tube (PMT) where it is mixed with 0.1 M carbonate buffer to initiate CL (Hamamatsu HC135 PMT, 900 V, 400 ms integration). This system requires 50 seconds for each H_2O_2 measurement and a limit of detection of 350 pM for open ocean seawater is reported by King et al.[32] Instead of adding an acid wash loop to the injection valve to prevent interference of precipitated $MgOH_2$ at high pH,[32] we decreased the carbonate buffer pH to 10.4 and used 0.2 M HCl as the carrier, which also helped decrease background CL. A 2 mM H_2O_2 stock solution was prepared from 30% H_2O_2 (J.T. Baker) and checked weekly using its absorbance at 240 nm and a molar absorptivity for H_2O_2 of 38.1 M^{-1} cm^{-1}.[33] Standards were prepared in aged seawater checked for low H_2O_2 against the same seawater with added catalase (20 µL of 100 units L^{-1} in 20 mL seawater: C100 Sigma-Aldrich). Under these conditions, the H_2O_2 detection limit, defined as three times the standard deviation of the blank, was 2.2 nM.

2.3.2 *Superoxide Analysis*: Superoxide was also measured using the FeLume system employing the chemiluminescent reaction between O_2^- and a methyl Cypridina luciferin analogue (2-methyl-6-(4-methoxyphenyl)-3,7-dihydroimidazo[1,2-a]pyrazin-3(7*H*)-one; MCLA; TCI America), following the methods of Rose et al.[34] and Garg et al.[35] In this case, no sample loop was used and both the seawater sample and chemiluminescent reagent were continuously delivered directly to the flow cell with a peristaltic pump (Rainin, 15 RPM). The PMT was operated at 1200V with an 800 ms integration time. The chemiluminescent reagent contained 2.45 µM MCLA in 0.5 M sodium acetate/50 µM diethylenetriaminepentaacetic acid (DTPA) solution, adjusted to pH 6 with

concentrated HCl. The conjugate base of MCLA ($MCLA^-$; pKa = 7.64 ± 0.03) also reacts with molecular oxygen to chemiluminesce,[36] giving an increased background signal due to the $MCLA^-/O_2$ reaction at basic pH. While acidic pH increases the reaction rate for MCLA with O_2^-,[37] it also increases the rate of uncatalyzed superoxide dismutation by about an order of magnitude for every unit decrease in pH. To prevent changes in signal due to changes in reaction temperature,[24] all seawater samples were brought to room temperature before each experiment. The enzyme superoxide dismutase (SOD; 200 U L^{-1} based on the manufacturer's assay; S5395-15KU Sigma) was added at the end of irradiation experiments (see Section 2.4.2) to observe the subsequent signal reduction to near pre-irradiation background levels. A stock solution of ~1.5 x 10^6 U L^{-1} SOD was prepared in Milli-Q and stored at 4 °C in the dark when not in use.

2.3.3 ***Superoxide System Calibration and Standards:*** Because of its instability in aqueous solutions, all methods that produce superoxide standards in μM concentrations are subject to their own analytical issues.[24] To calibrate the MCLA reaction in the FeLume system for each freshly prepared MCLA reagent, superoxide standards were generated via UV photolysis of acetone in an ethanol solution following modifications to the methods of McDowell et al.[38] and Ong.[39] A solution of 41 mM acetone, 6 M ethanol, 30 μM DTPA in 0.1 M borate buffer (pH = 12.5) was irradiated in a 1 cm quartz cell with a Hg lamp (Pen-Ray) for ≤30 seconds. The concentration of superoxide was monitored in real time using the absorbance at 240 nm and a O_2^- extinction coefficient (ε) of 2183 M^{-1} cm^{-1} corrected for the absorbance of H_2O_2 at 240 nm as described by Bielski[40] as follows

$$\varepsilon_{O2\text{- CORRECTED}} = \varepsilon_{O2\text{-}} - 0.5\varepsilon_{H2O2}\ M^{-1}\ cm^{-1} = 2183 \text{ at pH } 12.5 \quad (7)$$

It has been noted that DTPA breaks down in UV light and increases absorbance that can

interfere with O_2^- determination[24], but given the very short irradiation time required to generate O_2^- in our standard method, it is not likely that DTPA photolysis contributed significantly to the absorbance reading. When the superoxide reached about 100 μM, an aliquot was withdrawn and spiked into seawater samples containing 30 μM DTPA to eliminate metal catalyzed O_2^- decay.[18,41] Concentrations for O_2^- standards ranged from 5 - 50 nM ($[O_2^-]_0$) and were monitored by the FeLume for ~10 minutes. In un-amended, filtered seawater, O_2^- decay can be described with the following equation

$$\frac{-\mathrm{d}[O_2^-]}{\mathrm{dt}} = 2k_D[O_2^-]^2 + \sum k_M[M]_X[O_2^-] + k_{pseudo}[O_2^-] \quad (8)$$

where k_D is the is the pH and temperature dependent dismutation rate constant (derived from equation 4), k_M is the rate constant for the reaction of superoxide with metal species (M_x), and k_{pseudo} is the rate constant for the reaction of O_2^- with other sinks.[42] If all pseudo-first order decay terms are summed, or metal sink terms are eliminated with the chelator DTPA, then Equation 8 reduces to

$$\frac{-\mathrm{d}[O_2^-]}{\mathrm{dt}} = 2k_D[O_2^-]^2 + k_{pseudo}[O_2^-] \quad (9)$$

Integrating Equation 9 and assuming that the FeLume signal (S, corrected for background chemiluminescence) is directly proportional to O_2^- concentration ($S = C\,[O_2^-]$)[18,43,44], S is modeled as a function of time (t) with the following equation[18,35]

$$S = \frac{k_{pseudo}S_0}{k_{pseudo}e^{k_{pseudo}t} + k_D[O_2^-]_0(e^{k_{pseudo}t} - 1)} \quad (10)$$

where S_0 is the FeLume signal at time zero and $[O_2^-]_0$ is the spiked superoxide concentration. FeLume data was fit to Equation 10 with a non-linear regression of S vs. t using the curve fitting toolbox in MATLAB ®. The second order dismutation rate

constant, k_D, was calculated for each seawater sample using Equation 4[17] and pH values determined using a Ross Ultra, glass combination pH electrotrode (Thermo Scientific) calibrated with NBS standard buffers. Although calibrating seawater pH with Tris buffers of a similar composition to seawater (i.e. of a similar ionic strength) is recommended,[45] primary standards were used here for direct compatibility with the procedures of Zafiriou.[17] The pseudo-first order rate constant for catalyzed O_2^- decay (k_{pseudo}) and S_0 at the time of the spike were used as fitting parameters. The model fit observed O_2^- decay ($r^2 > 0.94$ for all decay curves, n = 9) giving a k_{pseudo} of $15 \pm 2 \times 10^{-3}$ s^{-1}, in good agreement with the k_{pseudo} of 6.6×10^{-3} s^{-1} for superoxide decay in non-irradiated solutions containing 1 mg L^{-1} Suwannee River fulvic acid (SRFA)[35] and the k_{org} of $9.3 - 15.6 \times 10^{-3}$ s^{-1} determined in tropical Atlantic water from 10 m.[43] A linear regression of S_0 vs $[O_2^-]_0$ gave a C value of 3.05×10^4 counts nM^{-1} ($r^2 = 0.90$, n = 9) which was used in subsequent O_2^- concentration determinations.

2.4 Photochemical Irradiations

2.4.1 ***Apparent Quantum Yield Experiments for H_2O_2:*** Photochemical experiments for H_2O_2 $\varphi(\lambda)$ determinations were performed using a Suntest CPS solar simulator equipped with a 1.5 kW xenon lamp (Atlas), as detailed in Johannessen and Miller.[30] Each seawater sample was brought to room temperature and partitioned into 15 gas-tight 10 cm cylindrical quartz spectrophotometric cells, filled and sealed with no headspace using caps fitted with Teflon faced, butyl rubber septa. The absorbance in each cell was measured from 250 – 800 nm both prior to and post irradiation and Milli-Q water was used as the absorbance blank. Raw absorbance spectra were corrected for scattering, the

difference in refractive index between salt water and the pure water blank, and instrument drift by fitting individual spectra to the equation:

$$A = Fe^{-S\lambda} + O \quad (11)$$

over the 680 – 800 nm range for CDOM measured in 10 cm spectrophotometer cells and over the 700-750 nm range for CDOM measured in 1 m pathlength LWCC[46] using the MATLAB ® nonlinear curve fitting routine *nlinfit*, where A (unitless) is absorbance, F is a fitting coefficient, S is the spectral slope coefficient, and O is the offset.[47] The offset was subtracted from the absorbance spectra, and any differences in absorbance spectra measured using the LWCC and the Lambda 40 were attributed to differences in the baseline offset. Because salt solutions have a higher refractive index than the freshwater on which instruments are blanked, seawater should show an apparent negative absorbance at certain wavelengths, an effect that can be exacerbated in the long pathlength LWCC.[46,48,49] This refractive index effect can be corrected by preparing blanks with a similar refractive index to the samples[48] or by employing an empirical salinity correction.[49] Our absorbance spectra determined using both instruments were comparable in the UV (<350 nm) to the extent that no significant alterations to our final apparent quantum yield calculation could be detected given the overall uncertainty of the multispectral AQY method. Corrected absorbance spectra were converted to Napierian absorption coefficient ($a_g(\lambda)$ (m^{-1})) with the equation:

$$a_g(\lambda) = \frac{\ln(10)A}{L} \quad (12)$$

over the 280 – 700 nm range, where L (m) is the pathlength of the spectrophotometric cell. Irradiations typically lasted 3 to 12 hours, and CDOM absorption spectra measured before and after irradiation were averaged for each cell for calculation but did not change

significantly.

Spectrophotometric cells were placed vertically in a black water-cooled aluminum irradiation block below the solar simulator, which maintained the cells at 20 °C and allowed no transfer of light between cells. Each cell was aligned under a variety of evenly spaced Schott long-band-pass cutoff filters (280, 295, 305, 320, 380, 425, and 480 nm). Since the irradiation block holds 15 cells, the setup included duplicate cutoff filters and a dark. The spectral downwelling irradiance entering each cell, $E_0(\lambda)$ (mol(photons) m^{-2} s^{-1} nm^{-1}), was quantified at 1 nm intervals with a UV-Vis portable spectroradiometer (OL756, Optronic Laboratories) fitted with a quartz fiber optic cable and integrating sphere, previously calibrated with a NIST standard lamp (OL 83A & OL220 lamp, Optronic Laboratories). Photons absorption rate by CDOM, $Q_a(\lambda)$ (mol(photons) s^{-1} nm^{-1}), in each sample was calculated following the recommendations of Hu et al.[50], correcting for self-shading via the equation:

$$Q_a(\lambda) = E_0(\lambda)S(1 - e^{-a_g(\lambda)L})t \quad (13)$$

where S (m^2) is the surface area of the irradiated cell and t (s) is irradiation time.

The H_2O_2 production rate is equal to the product of the H_2O_2 $\varphi(\lambda)$ and $Q_a(\lambda)$:

$$\frac{d[H_2O_2]}{dt} = \phi(\lambda)Q_a(\lambda) \quad (14)$$

allowing for the determination of $\varphi(\lambda)$. The spectral quantum yield for each sample is modeled from the H_2O_2 production rate and $Q_a(\lambda)$ with the following equation:

$$\phi(\lambda) = e^{-(m_1 + m_2(\lambda - 290))} \quad (15)$$

The fitting parameters (m values above) were again determined using the MATLAB ® nonlinear curve fitting routine, *nlinfit* (Table 1A).

2.4.2 *Photochemical Superoxide Kinetic Experiments:* All photochemical superoxide experiments were carried out on fresh 0.2 μm filtered surface seawater collected in the Gulf of Alaska aboard the *R/V Mellville*. Samples were irradiated under the solar simulator in acid-cleaned and Milli-Q rinsed 600 mL jacketed beakers (Ace Glass) covered with quartz glass. Two crossed glass rods and a Teflon stir bar ensured turbulent mixing and all samples were maintained at 20 °C with a recirculating water bath. O_2^- concentrations were monitored with MCLA chemiluminescence both during and post irradiation to observe O_2^- steady-state concentrations ($[O_2^-]_{ss}$) and decay kinetics respectively. Typically, samples were irradiated about 30 minutes, to ensure $[O_2^-]_{ss}$ had been reached. Post irradiation, FeLume signal, and thus O_2^- decay, were again described by Equations 9 and 10, effectively combining metal sinks and all other first order sinks into the k_{pseudo} term.

2.5 Model for Photochemical Rate Estimates from Satellite Data

Our general methods for estimating the photochemical production rate of H_2O_2 in the surface ocean from remotely sensed satellite data very closely follow the approach of Fichot and Miller[26] for global estimates for CO photoproduction. For full details regarding application, assumptions, and error analysis for retrieval of UV attenuation data from SeaWiFS imagery using the original *SeaUV* algorithms and implementation of this optical data for photochemical calculations on global scales, the reader is referred to the original publications.[26,51] We implemented the "practical" model (section 2.1.2, equation (4), Fichot and Miller[26]) with the published assumptions that the 290-490 nm spectral range captures photochemical activity, that upwelling scalar irradiance can be ignored,

and that the attenuation of downwelling scalar irradiance can be described by $K_d(\lambda)$. This approach was used to determine total H_2O_2 photoproduction rates (P_{H2O2}; mol(H_2O_2) m^{-3} d^{-1}) with the equation:

$$P_{H_2O_2} \approx \int_{290}^{490} E_{0d}(\lambda,0^-)e^{-K_d(\lambda,z)}a_g(\lambda,z)\phi(\lambda,z)d\lambda \quad (16)$$

Knowledge of $\varphi(\lambda)$, $a_g(\lambda)$, and the *in situ* light field obtained from the downwelling scalar irradiance just below the surface ($E_{0d}(\lambda,0^-)$) and the average $K_d(\lambda)$ for the depth range in question, allows the photochemical production rate to be calculated for any depth (z; m) or depth interval (Equation 16).

2.5.1 ***Retrieving Optical Parameters for Global Photochemical Model***: Fichot et al.[51] published a set of algorithms (*SeaUV*/*SeaUV*$_C$) for retrieving $K_d(\lambda)$ from SeaWiFS normalized water-leaving radiance ($nLw(\lambda)$) with an estimated overall accuracy of ±15-20% based on comparison to Hydrolight-modeled and *in situ* $K_d(\lambda)$ measurements. Fichot and Miller[26] subsequently used the *SeaUV* model retrievals of $K_d(\lambda)$ with $a_g(\lambda)$ data to estimate global, depth-resolved photochemical fluxes of CO as a demonstration of the model's application. Briefly, our implementation of this approach is outlined as follows.

The *SeaUV* algorithms were used to retrieve $K_d(\lambda)$ at 320, 340, 380, 412, 443 and 490 nm from the last 7 years of SeaWiFS monthly data (2003 –2010) and binned to create monthly average climatologies for the global ocean with a spatial resolution of 40 x 40 *cos*(latitude) and a grid size of 500 x 1000 pixels. Spectrally resolved $K_d(\lambda)$ (320 – 490 nm) was determined with a cubic interpolation and extended into the UVB (290 – 320) with a spectral slope coefficient determined between $K_d(320)$ and $K_d(340)$. Full $a_g(\lambda)$ spectra were calculated assuming a $a_g(320)/K_d(320)$ ratio of 0.68 and a spectral slope coefficient, S_{ag}, of 0.0194[26] with the following equation:

$$a_g(\lambda) = a_g(320)e^{(-S_{a_g}(\lambda-320))} \quad (17)$$

To supply $E_{0d}(\lambda, 0^-)$ for the photochemical model, we started with modeled global clear-sky downwelling irradiance reaching the earth's surface from 280 to 700 nm at 1 nm intervals using the System for Transfer of Atmospheric Radiation (STAR).[52] Model inputs included monthly average total ozone concentrations from the Total Ozone Mapping Spectrometer (TOMS) and oceanic values for aerosol, humidity, etc. as described in Fichot and Miller[26] and a cloud correction for solar irradiance at the sea surface was obtained using monthly averaged TOMS UV reflectivities from 1996 to 2003. The final product from this model is a 7-year climatology for cloud-corrected, daily-integrated, downwelling scalar irradiance, $E_{0d}^{Day}(\lambda, 0^-)$, at the sea surface for the 15th of each month. By combining STAR-modeled $E_{0d}^{Day}(\lambda, 0^-)$ with $K_d(\lambda)$ retrieved with *SeaUV* and $a_g(\lambda)$ estimates, and assuming the these optical properties do not vary over the temporal and spatial scales of the calculation, we mapped monthly climatologies for average daily photon absorption rates and used them in subsequent photochemical calculations (e.g. Equation 16).

2.5.2 ***Retrieving Temperature for Global Photochemical Model:*** There is clear evidence that a significant portion of observed natural variability in H_2O_2 photoproduction is temperature dependent.[19] This is expected given the secondary thermal reactions (Equations 1 - 4) that control H_2O_2 formation following primary photochemical CDOM reactions with oxygen. Activation energies (E_a), determined by Kieber et al.[19] using an Arrhenius plot are similar between 295 and 370 nm, giving an average value of 21.8 kJ mol^{-1}. Therefore, to better implement our global photochemical production model, H_2O_2 spectral $\varphi(\lambda)$ values determined at 20°C (Section 2.4.1) were corrected for temperature-

dependence with the equation:

$$\ln\frac{\phi_{\lambda,T}}{\phi_{\lambda,298}} = \frac{21.8}{R}\left(\frac{1}{298} - \frac{1}{T}\right) \quad (18)$$

where $\varphi_{\lambda,T}$ is the wavelength-temperature-dependent AQY, $\varphi_{\lambda,298}$ is the AQY at 298 K, R is the universal gas constant (8.3145 x 10^{-3} kJ K^{-1} mol^{-1}), and T is temperature (K).[19] For more accurate global mapping of photochemical H_2O_2 production, Level 3 global monthly-binned daytime SST data from MODIS Aqua, with a spatial resolution of 4.63 km, were averaged from 2003 to 2010 to create monthly climatologies for the global ocean and fit to a grid size of 500 x 1000 pixels to match the modeled solar irradiances and the outputs from the *SeaUV* model ($K_d(\lambda)$ and $a_g(\lambda)$). The matched T value retrieved at each pixel was then used in Equation (18) to modify the entire H_2O_2 $\varphi(\lambda)$ spectra for use in H_2O_2 photoproduction rates (Equation 16). Daytime SST products are susceptible to contamination from reflected sunlight but are still considered accurate to ± 0.4 °C.[53] Limitations inherent in using an average activation energy are discussed in Section 3.2 below.

3. RESULTS and DISCUSSION

3.1 H_2O_2 Apparent Quantum Yield Spectra

Given that the optical components of the practical model (Equation 16) are derived from *SeaUV* and STAR as described in the preceding sections, this leaves our selection of H_2O_2 AQY ($\varphi(\lambda)$) as a critical, yet somewhat subjective choice that contributes significant control over photoproduction estimates. Here we have based our selection on an evaluation of our laboratory irradiation results performed on both clear,

oceanic and dark, coastal surface samples (Table 1A) in comparison with reported spectral AQY for H_2O_2 available in the literature.

Our laboratory determined H_2O_2 AQY spectra decreased by about an order of magnitude over UV wavelengths, ranging from 1.41 – 10.0 x 10^{-4} at 290 nm to 0.15 – 1.34 x 10^{-4} at 400 nm (Table 1A, Figure 1). These are in reasonable agreement with AQY data determined for the Antarctic at 0 °C (7.4 x 10^{-4} at 290 nm to 0.1 x 10^{-4} at 400 nm[21]), for marine (coastal and open ocean) stations at 25 °C (3.56 – 10.4 x 10^{-4} at 290 nm to 0.17 – 0.97 x 10^{-4} at 400 nm[19]), and coastal sites at 30 °C (4.7 x 10^{-4} at 290 nm[15]). Yocis et al.[21] and Kieber et al.[19] compared apparent quantum yield data for H_2O_2 photoproduction from a variety of freshwater and marine samples and found that the $\varphi(\lambda)$ was quite similar for all regions studied. Yocis et al.[21] additionally determined H_2O_2 quantum yield spectra at 20°C in Antarctic samples, which increased the $\varphi(\lambda)$ for H_2O_2 by about a factor of 3 (22 x 10^{-4} at 290 nm) over the same samples at 0 °C. These AQY spectra are comparable to H_2O_2 quantum yield data determined in VH Pond and Newman's Lake, FL (6.6 and 15 x 10^{-4} at 300 nm[54]), in the Orinoco River outflow (8.95 – 13.6 x 10^{-4} at 300 nm[55]), and in 1:5 diluted Shark River water (6.9 x 10^{-4} at 300 nm[20]). The AQY spectra we determined for our clearest open ocean samples (GOM4, GOA1, and GOA2, Table 1A) in this study, however, are generally lower than those determined in freshwater systems (Figure 1). O'Sullivan et al.[15] observed a similar result, reporting H_2O_2 quantum yield values at the lower range of those determined for the Orinoco River outflow by Moore et al.[55] In fact, the AQY spectra determined in our open ocean water samples agree best with those determined for the oligotrophic Antarctic[21,23] and for Station ALOHA,[23] suggesting that there may be differences in the efficiency for H_2O_2

415 photoproduction between terrigenous and marine CDOM sources (Figure 1).

416 Some progress has been made in understanding the mechanisms involved in the
417 photoproduction of H_2O_2 from CDOM. O'Sullivan et al.[15] observed a linear correlation
418 between H_2O_2 production and CDOM photobleaching and Dalrymple et al.[56] found a
419 strong correlation between the H_2O_2 AQY and the E2/E3 ratio (CDOM absorbance at 254
420 nm divided by that at 365 nm), a property correlated to DOM molecular weight.[57]
421 Through a detailed mechanistic investigation of photochemical H_2O_2 production from
422 humic substances and CDOM, Zhang et al.[14] concluded that charge transfer states,
423 aromatic ketones and aldehydes, $^1O_2$, and excited triplet states of quinones do not
424 contribute significantly to H_2O_2 production. More work is needed to determine whether
425 these relationships hold true in samples primarily containing marine DOM. In marine
426 samples, and in the open ocean in particular, H_2O_2 AQY spectra are generally very
427 similar and their variability is controlled mainly by differences in temperature.[19,21]

428 To best reflect the oligotrophic waters that dominate the global ocean, we
429 determined a pooled quantum yield spectrum, calculated by fitting Equation 15 to all
430 H_2O_2 production data (n = 26) measured for irradiation experiments done in the Gulf of
431 Alaska (Samples GOA1 and GOA2), resulting in the following equation

432 $$\phi(\lambda)_{\text{pooled}} = e^{-(8.201+0.0238(\lambda-290))} \quad (19)$$

433 This result was used as input for subsequent global photochemical calculations (Equation
434 16). Although GOM4 is also an open ocean sample, data from this irradiation were
435 excluded from the pooled AQY fit because of its poor agreement between measured
436 H_2O_2 production and that predicted from its individual AQY spectrum ($r^2 = 0.75$). The
437 pooled quantum yield values determined here are about 2 times lower than the Kieber et

438 al.[19] average AQY value at 290 nm (adjusted to 20°C as described in Section 2.5.2;
439 Figure 1) and 1.4 times lower than the average AQY value at 400 nm, determined for a
440 variety of marine waters (coastal through open ocean). Because the H_2O_2 quantum yield
441 spectrum used in our model is at the lower end of published AQY spectra (Figure 1), we
442 consider our estimates of P_{H2O2} determined in Section 3.2 below to be minimum rates for
443 the open ocean.
444
445 **3.2 Global Photochemical H_2O_2 Flux Estimates**
446 With the additional temperature modification for the pooled H_2O_2 AQY
447 spectrum, global distributions of surface ocean P_{H2O2} were calculated for each month at a
448 depth of 1 m and were converted to nM d^{-1} from mol(H_2O_2) m^{-3} d^{-1} to compare to
449 literature values (Table 2). Open ocean production rates ranged from <1 to over 100 nM
450 d^{-1}, with a yearly global average of ~45 nM d^{-1}. Spatial and temporal variability in P_{H2O2}
451 is shown in Figure 2B using the months of January, April, July, and October as examples.
452 Considering the potential errors associated with retrieving seawater optical properties
453 from satellite data, Fichot and Miller[26] demonstrated that the *SeaUV* [51] algorithm provides
454 a relatively good approximation of UV-visible photon absorption rates in the open ocean.
455 However, as noted in Fichot and Miller,[26] the use of a single quantum yield spectrum
456 does not have the capacity to capture the underlying processes controlling the known
457 variability in AQY spectra (Figure 1), limiting the complete understanding of the
458 magnitude and distributions of H_2O_2 photoproduction rates in surface seawater.
459 Therefore, spatial and temporal distributions of calculated photoproduction rates only
460 track with sea surface temperature and solar irradiation absorption rates.

461 Perhaps surprisingly, H_2O_2 photoproduction rates determined from our global 7-
462 year climatologies are in reasonable agreement with discrete H_2O_2 production
463 measurements. In a free floating drifter study, Kieber et al.[19] measured gross P_{H2O2} of 72
464 nM d^{-1} for an oligotrophic station in the northwest Atlantic in the summer. To compare,
465 P_{H2O2} was 63 nM d^{-1} at 40N 70W on our July map. Yocis et al.[21] measured gross P_{H2O2}
466 rates of 2.5 – 3.5 nM h^{-1} in Antarctic waters in the summer. Assuming a 12 h
467 deployment, these rates are on the order of 25 – 37 nM d^{-1}, similar to the 32.5 nM d^{-1}
468 estimated at 55S 55W on our December map. Figure 3 shows daily H_2O_2
469 photoproduction rates averaged for the year are highest in equatorial regions and lowest
470 at the poles (range: 0.07 - 93.2; average: 40.4; median; 39.5 nM d^{-1}). When summed over
471 the entire year, this amounts to an average of about 8 μM yr^{-1} and near 30 μM yr^{-1} in
472 productive regions. The reader is reminded however, that these data are calculated from
473 7-year average global climatologies and the comparisons made here are meant to show
474 the applicability of our model, and by no means represent an attempt at validation with
475 measured *in situ* H_2O_2 photoproduction rates.

476 Although the use of a single AQY spectrum has known limitations, it does
477 allow for a direct assessment of the temperature dependence on photochemical H_2O_2
478 production rates. If the pooled H_2O_2 AQY spectrum (Equation 19) is not adjusted for
479 temperature (Figure 2A), production rates are underestimated in equatorial regions and
480 overestimated in polar regions when compared to production rates calculated with
481 temperature modified AQY spectra (Equation 18, Figure 2B), thereby underestimating
482 average global monthly photoproduction rates by ~3 – 9%. The difference is even more
483 striking in monthly maximum production rates, which are underestimated by ~15 – 25%

when not accounting for the temperature dependence on the H_2O_2 AQY spectrum. Estimates of P_{H2O2} determined at 40N 70W in July drop from 63 nM d^{-1} to 59 nM d^{-1} and at 55S 55W in December increase from 32.5 nM d^{-1} to 49.1 nM d^{-1}, creating greater deviations from *in situ* rates discussed above.[19,21]

While the studies cited in Section 3.1 above have improved our understanding of mechanisms involved in H_2O_2 production from the photoexcitation of CDOM, the fact that H_2O_2 production is a result of a thermal reaction is greatly ignored. Kieber et al.[19] represents the first attempt at simultaneously understanding the temperature and wavelength dependence of H_2O_2 photochemistry. The E_a determined by Kieber et al.[19] ranges from 8.3 to 52.7 kJ mol^{-1}, with the largest difference in E_a between 290 and 400 nm (average E_a values increased from 16.6 to 31.9 kJ mol^{-1}). Further investigation into the apparent variability in E_a with excitation wavelength will improve estimates of H_2O_2 photoproduction rates, which is pressing when considering rising sea surface temperatures in the ocean. Results from Kieber et al.[19] demonstrated that a 10 °C increase in seawater increased H_2O_2 AQY spectra by a factor of about 1.8 on average. In order to predict the effect of a warmer future ocean, we applied a uniform 5 °C increase to our monthly SST climatologies. When these "future" SST maps were used to modify the pooled H_2O_2 AQY spectrum, H_2O_2 photoproduction rates increased by 16% on average (Figure 2C). This does not necessarily mean that *in situ* H_2O_2 will change in the same regard, especially if the rates of H_2O_2 decay increase as well in a warmer ocean. Steingenberger and Croot[58] found a negative correlation between H_2O_2 concentration and SST, attributing the effect to higher enzymatic sink strength for H_2O_2 at higher temperatures. In a future scenario where P_{H2O2} increases by 16%, biological decay will

most certainly increase as well. Although it is unclear how biology will respond to an increased P_{H2O2}, it is clear that organisms will have to adjust the metabolic energy required to counter the increased rate of H_2O_2 photoproduction.

3.3 Global Superoxide Steady-State Estimates

While AQY spectra determined here and implemented in our model are for H_2O_2, in reality, thermal reactions involving superoxide control its formation. Although it is vitally important to quantify superoxide distributions and photoproduction rates on a global scale in order to understand its role in biogeochemical cycles, determining O_2^- photoproduction rates from that for H_2O_2 is not a simple task. Presently, the extension of our photochemical H_2O_2 production model to include estimates of global O_2^- photoproduction rates and $[O_2^-]_{ss}$ in the surface ocean remains highly speculative, primarily due to incomplete understanding of the mechanisms regulating O_2^- formation and decay. The following sections, therefore, outline the approach taken and justifications for the choices we made to best estimate spatial and seasonal distributions of superoxide dynamics in the open ocean.

3.3.1 ***Global Photochemical Superoxide Steady-State Estimates assuming Dismutation as the Dominant Sink:*** At steady-state, superoxide production and loss terms must balance. As a simplified first approach, we estimated open ocean $[O_2^-]_{ss}$ assuming biomolecular dismutation is the only sink for O_2^-. There is evidence that H_2O_2 production in natural waters can be explained primarily by O_2^- dismutation.[35,59] Therefore, in making this assumption, Equation 9 reduces to:

$$\frac{-\mathrm{d}[O_2^-]}{\mathrm{dt}} = 2k_D[O_2^-]^2 \qquad (20)$$

The stociometry of superoxide dismutation (Equation 1 or 2) predicts $0.5H_2O_2$ per O_2^-, implying that

$$P_{O_2^-} = 2P_{H_2O_2} \quad (21)$$

and $[O_2^-]_{ss}$ can be estimated on a global scale with Equation 22 below

$$[O_2^-]_{ss} = \left(\frac{P_{O_2^-}}{2k_D}\right)^{0.5} = \left(\frac{P_{H_2O_2}}{k_D}\right)^{0.5} \quad (22)$$

Since superoxide exists as either HO_2 or O_2^-, the overall dismutation rate constant (k_D) was calculated at an average oceanic pH of 8.2 from the rate constants for reactions 1 and 2[16] and the K_a for HO_2 (4.6 ± 0.15 in seawater[17]). Therefore, the overall dismutation rate constant for superoxide decay can be expressed as:

$$k_D = \frac{k_2[H^+]^2 + k_1 K_a[H^+]}{(K_a + [H^+])^2} \quad (23)$$

Rate constants calculated using this method are in good agreement with those calculated by Zafiriou[17] for superoxide dismutation in seawater. Second order O_2^- decay is highly pH dependent and a decrease of just 0.4 pH units, from 8.2 to 7.8, increases k_D from 2.43 to 6.11×10^4 M^{-1} s^{-1}. We also adjusted k_D for changes in temperature assuming that the average E_a determined by Kieber et al.[19] for H_2O_2 AQY spectra could also be applied to k_D (Equation 18).

Using temperature and pH modified k_D in conjunction with our global models of P_{H2O2} only allows for calculation of daily-integrated $[O_2^-]_{ss}$ values. These integrated values are misleading however because $[O_2^-]_{ss}$ changes dramatically with the intensity of the sun throughout the day. It is therefore more appropriate to calculate steady-state concentrations at a certain time of day. We chose to examine midday $[O_2^-]_{ss}$ because

superoxide concentrations should be highest at solar noon. We modeled daily-integrated H_2O_2 photoproduction as a sine curve with the equation:

$$P_{H_2O_2}(\text{daily-integrated}) = A\int_0^{t_{end}} \sin(2\pi ft)\text{dt} \quad (24)$$

where $A = P_{H2O2}(\text{at midday}) = \pi P_{H2O2}(\text{daily-integrated})/(2t_{end})$, $f = 1/(2t_{end})$, t is the time of day and t_{end} is the length of day. For our global climatologies, t_{end} was calculated as a function of latitude for the 15th of each month. Solving for midday H_2O_2 and O_2^- production rates yields the following modification to Equation 22:

$$[O_2^-]_{ss}(\text{midday}) = \left(\frac{\pi P_{H_2O_2}(\text{daily-integrated})}{2t_{end}k_D}\right)^{0.5} \quad (25)$$

Global distributions of midday $[O_2^-]_{ss}$ were modeled for the 15th of each month using a SST-modified k_D at a pH of 8.2, showing October as an example in Figure 4. In general, $[O_2^-]_{ss}$ values are highest in equatorial regions and lowest in the poles ranging from ~0.1 – 5 nM, with a yearly average of about 2.6 nM. In order to examine changes in $[O_2^-]_{ss}$ in a future ocean that is not only warmer but also more acidic, midday $[O_2^-]_{ss}$ concentrations were recalculated with an increased SST and a decreased pH. k_D and $\varphi(\lambda)$ were again modified with Equation 18, but increasing SST by 5 °C did not change the $[O_2^-]_{ss}$ determined with our model because, having no other direct data to consider, we assumed both the rates of superoxide photoproduction *and* it's loss can be adjusted using the same activation energy. However, when the pH was decreased the resulting $[O_2^-]_{ss}$ concentrations at pH 7.8 were ~55% lower than those calculated at pH 8.2 (Figure 4).

3.3.2 ***Investigating Superoxide Decay via Pathways other than Dismutation:*** The steady-state O_2^- concentrations modeled by assuming that dismutation is the dominant sink are higher than those reported for the surface equatorial Pacific (~220 pM)[60] and the

Gulf of Alaska (~ 550 pM)[41] even though neither fully reflect the photochemical source, having been removed from UV light prior to measurements. Other estimates that use dismutation alone have also overestimated $[O_2^-]_{ss}$ by about 7 – 8 nM.[17,61] This most likely results from ignoring additional sinks of superoxide. To this point, some observations have successfully modeled superoxide decay via a pseudo-first order rate law, and not the second order fit required by dismutation.[18,62] To determine the best approach for our calculations, we irradiated surface seawater in the Gulf of Alaska until a $[O_2^-]_{ss}$ was measured, shut off the lamp, and measured the subsequent O_2^- signal post-irradiation. The resulting O_2^- decay was modeled according to Equation 10, as described in Section 2.3.3. The pseudo-first order rate constants determined from our irradiation experiments ranged from 1.7 to 4.6 x 10^{-3} s^{-1} (Table 1B), in good agreement with pseudo-first order rate constants for O_2^- decay determined in the Equatorial Pacific in the presence of DTPA (<10^{-4} to 9.7 x 10^{-3} s^{-1})[60] and the Southern Ocean (6 ± 1 x 10^{-3} s^{-1}).[18] These results are consistent with the probability that a large portion of O_2^- in oligotrophic waters decays via pathways other than dismutation.

Given the fact that O_2^- can act as both an oxidant and a reductant, the potential decay mechanisms in seawater are complex. Figure 5 presents a compilation of generic superoxide decay pathways, showing the modeling approach of describing the non-dismutation pathways using a single rate constant, k_{pseudo}. If catalytic O_2^- decay is irreversible, then the amount of H_2O_2 generated per O_2^- should be between 0 and 1, and in fact the ratio has been calculated in coastal seawater to be around 0.6 – 0.75 H_2O_2 per O_2^-.[63] On the other hand, a catalytic redox cycle, (i.e. the dashed lines connecting paths (2) and (3) in Figure 5), would produce 0.5 H_2O_2 per O_2^- consumed, and maintain the 2:1

596 stoichiometric ratio between P_{O2^-} and P_{H2O2} typical of dismutation. This catalytic cycling
597 is consistent with results reported for coastal seawater[42] and 1 mg L^{-1} SRFA solutions,[35]
598 but it is unclear whether or not this is a valid assumption for the open ocean. Recently,
599 Wuttig et al.[64] found H_2O_2 production rates that were about half the O_2^- production rates
600 generated by a thermal superoxide source[24] in open ocean seawater. However,
601 considering other possible reactions that occur between superoxide and excited state
602 CDOM *in situ*, it has not been determined whether this ratio is true of H_2O_2 produced
603 photochemically. Furthermore, Micinski et al.[59] suggested that O_2^- dismutation accounts
604 for nearly all photochemical H_2O_2 production based on measured O_2^- production rates in
605 the eastern Caribbean. However, there was large variability in P_{O2^-} (0.1 – 6 nM min^{-1}
606 spring; 0.2 – 8 nM min^{-1} fall) and P_{H2O2} measured during the same field campaigns (0.39
607 ± 0.19 nM min^{-1} spring, 2.23 ± 1.5 nM min^{-1} fall)[55] suggesting that for the open ocean, it
608 is possible that the stoichiometric relationship between P_{H2O2} and P_{O2^-} may not simply be
609 described using a factor of two.

610 For this reason, we compared H_2O_2 produced in irradiated filtered seawater with
611 and without additions of the enzyme superoxide dismutase (SOD) to help clarify existing
612 pathways in our open ocean model. Since SOD catalyzes O_2^- disproportionation at a rate
613 $>10^9$ M^{-1} s^{-1},[64] when present, essentially all superoxide proceeds through the dismutation
614 path (1) to H_2O_2. Following the recommendations of Garg et al.,[35] SOD at 200 U L^{-1} was
615 added to open ocean surface seawater samples from the Gulf of Alaska (GoA1&2 Table
616 1). These samples were irradiated side by side in the solar simulator in 600 mL jacketed
617 beakers at 20 °C with quartz lids for up to 3 hours. For these samples, H_2O_2
618 photoproduction in the presence of SOD was indistinguishable from that produced in its

absence (Figure 6). Shaked et al.[62] also observed that SOD had no effect on H_2O_2 photoproduction in the Gulf of Aqaba. Additionally, based on O_2^- steady-state measurements during irradiation experiments and modeled pseudo-first order O_2^- decay constants in the dark, Shaked et al.[62] also calculated P_{O2-} ranging from 3 – 25 pM s^{-1} and P_{H2O2} ranging from 4 – 10 pM s^{-1}. Their results suggest that the P_{O2-}:P_{H2O2} of 2:1 is a reasonable estimate in seawater, but the authors note that a 1:1 ratio cannot be ruled out.

A direct approach to establishing this stoichiometric relationship is to monitor both P_{H2O2} and P_{O2-} at the same time in the same sample. Rusak et al.[66] have done this during irradiations of unfiltered water collected east of New Zealand, reporting P_{H2O2} and P_{O2-} to be 28 pM min^{-1} and 76 pM min^{-1}, respectively, giving a P_{O2-}:P_{H2O2} of 2.7:1 possibly due to H_2O_2 loss in unfiltered water. However, during 20 minute irradiations of filtered seawater, Rusak et al.[66] also saw P_{O2-} decrease while P_{H2O2} increased, an ambiguous result that points out the current poorly constrained relationship between P_{H2O2} and P_{O2}. Based on our laboratory results and with limited research into the ratio of P_{H2O2} to P_{O2-}, it seems that in clear, open ocean surface waters, an oxidative pathway (2) for O_2^- is negligible , and depending on the relative strengths of reductive catalysis (3) and dismutation (1), the P_{O2-}:P_{H2O2} is somewhere between 1 and 2. It is also apparent that until significantly more information on the photo-efficiency of O_2^- production becomes available, estimates of P_{O2-} based on hydrogen peroxide production will remain ill-defined.

3.3.3 ***Global Photochemical Superoxide Steady-State Estimates Including Additional Sinks for Superoxide:*** In addition to our work in the Gulf of Alaska, there are only a few studies on superoxide decay kinetics in the open ocean.[18,41,43,60] In these studies, DTPA

642 was used to examine decay kinetics in seawater[18,43,60] but all use different chelator
643 concentrations and pre-equilibration times, making the selection of a literature value for
644 use in superoxide decay models in the open ocean difficult. Because biomolecular
645 dismutation kinetics for superoxide are well defined as a function of temperature and
646 pH[16,17] we included the additional term for combined catalytic decay, k_{pseudo} (Equation 9),
647 in our model to improve estimates of $[O_2^-]_{ss}$ in the surface ocean. For our open ocean
648 model, we chose an average k_{pseudo} value of $2.6 \pm 1.4 \times 10^{-3}$ s^{-1}, determined from
649 irradiation experiments done at sea on freshly collected surface seawater from the Gulf of
650 Alaska as described in Section 2.4.2 (Table 1B). Using this average value for k_{pseudo} is an
651 oversimplification of the complexity inherent in O_2^- dynamics in the open ocean because
652 it does not include metal rate constants and therefore the effects of seawater pH and ionic
653 strength on metal oxidation are lost. However, until we better understand the specific
654 mechanisms involved in a variety of oceanic environments and can make reasonable
655 estimates of trace metals, it remains a defendable choice for this initial attempt to model
656 $[O_2^-]_{ss}$ in the surface ocean from space.

657 Because a little bit of mystery remains in defining a universal relationship
658 between P_{H2O2} and P_{O2-}, our subsequent estimates are still made assuming that superoxide
659 photoproduction rates are twice that of hydrogen peroxide photoproduction rates.
660 Superoxide decay can be modeled by solving Equation 9, and $[O_2^-]_{ss}$ can be estimated at
661 midday as

662 $$[O_2^-]_{ss}(\text{midday}) = \frac{-k_{pseudo} + \left[k_{pseudo}^2 + \left(8\pi k_D P_{H_2O_2}(\text{daily-integrated})/t_{end}\right)\right]^{0.5}}{4k_D} \quad (28)$$

Further, even though the temperature dependence of k_{pseudo} is not known, for our steady-state estimates, we assumed the same temperature correction to k_{pseudo} that we applied to k_D and $\varphi(\lambda)$ (Equation 18). Additionally, because the effect of pH on k_{pseudo} was not determined here, we could not adjust k_{pseudo} for a change in pH. Despite these limitations, this model attempts to involve all the known superoxide decay kinetics for a more realistic estimate of $[O_2^-]_{ss}$, and results in concentrations reduced by a factor of about 20 (Figure 4). In addition to over an order of magnitude drop in concentration, $[O_2^-]_{ss}$ becomes less variable when compared to both modeled month-to-month average values and maximum midday concentrations. This implies that globally, k_{pseudo} is the dominant sink term for O_2. To check this line of reasoning, we recalculated $[O_2^-]_{ss}$ at midday using k_D climatologies determined at pH 7.8. Instead of reducing $[O_2^-]_{ss}$ by 55%, the inclusion of k_{pseudo} reduced $[O_2^-]_{ss}$ by only ~0.5%. These observations again stress that uncatalyzed dismutation is not the major pathway for superoxide in the open ocean.

3.4 Considerations for Future Remote Sensing Estimates Relating H_2O_2 & O_2^-

Presently, using our modeled P_{H2O2} to estimate $[O_2^-]_{ss}$ in the surface ocean is speculative due to insufficient knowledge of the specific mechanisms and kinetic pathways that regulate O_2^- formation and decay. However, this modeling exercise has identified several necessary assumptions and correction terms that will be required to more accurately estimate superoxide dynamics from data on H_2O_2. One key issue when addressing global ROS distributions is the assumption that P_{O2-} is twice that of P_{H2O2}, and this needs to be verified for oligotrophic water systems. While measuring P_{H2O2} and P_{O2-} simultaneously is useful, current reports are for only a few locations and do not reflect the

686 diversity that exists in a variety of marine waters. The best way to model P_{O2-} in
687 seawater would involve direct measurements of the AQY spectra for O_2^- in representative
688 water types. Until we understand and constrain the photo-efficiency for O_2^- production,
689 we cannot accurately predict P_{O2-} on a global scale.

690 As confirmed here and elsewhere, biomolecular dismutation is not the major
691 sink for superoxide in the open ocean.[18,41,60] Therefore, the multiple first-order pathways
692 for superoxide decay need to be accurately incorporated into the overall kinetic model. A
693 compilation of O_2^- data from open ocean environments and a standardization of sample
694 treatments for use in models will help immensely in this regard. For example, pseudo-
695 first order decay rate constants have been determined in a variety of marine waters by
696 adding known quantities of a superoxide standard to seawater (either as KO_2 or a
697 photochemical standard) and monitoring the subsequent chemiluminescence signal.[18,43,66]
698 In these studies, however, spiked superoxide ranged from about 50 to 100 nM, well
699 higher than *in situ* concentrations. While some studies suggest that this is not a
700 problem,[24] with elevated O_2^- levels, and given the typically low nM reactant
701 concentrations involved in open ocean ROS reactions, it is possible that measured decay
702 rates may be altered. Perhaps indicating a dependence of decay pathway distribution on
703 initial O_2^-, the k_{pseudo} values we determined for 25 – 42 nM spikes of the photochemical
704 standard into Gulf of Alaska samples were about 4 – 10 times higher than k_{pseudo} values
705 determined post-irradiation, typically starting at $[O_2^-]_{ss} \approx 2$ nM (unpublished data).
706 Therefore, it may be difficult to equate pseudo-first order decay kinetics determined from
707 superoxide spikes to those appropriate for naturally occurring conditions. Unfortunately,
708 there have only been a few shipboard studies measuring the decay of O_2^- concentrations

that are representative of the open ocean.[41,66] Without conclusive data on superoxide decay kinetics at ambient superoxide concentrations, it has been hard to figure out the best decay terms for use in $[O_2^-]_{ss}$ estimates based on remotely derived estimates of P_{H2O2}.

When attempting to understand the overall magnitude of superoxide decay as it relates to hydrogen peroxide formation, it is also essential to know the specific sink terms that control O_2^- decay. The observed pseudo-first order decay rate constants determined here represent the sum of all first order reaction rates. To accurately describe O_2^- decay in the open ocean, we now understand that not only is the magnitude of k_{pseudo} likely to change according to what drives O_2^- decay in different marine environments, but the stoichiometry of H_2O_2 production could change as well. Researchers have made a great deal of progress in recognizing the reactivity of superoxide with metals and organic matter. However, the rates for specific sink terms that control superoxide in seawater remain elusive. Heller and Croot[18] spiked ~50 nM of O_2^- standard into unamended seawater, as well as samples with added Cu, Fe or DTPA. Shaked et al.[62] performed a very similar experiment with sub- to low-nM concentrations of O_2^-. By observing O_2^- decay in all of these treatments, both groups found Cu to be a major sink for O_2^- in both the Southern Ocean and the Gulf of Aqaba. Recently, Wuttig et al. [13] performed a similar experiment in the eastern tropical North Atlantic, but also included additions of Mn to seawater, finding that Mn and organics were the primary sinks for O_2^- in that region. Further mechanistic studies like this will increase our confidence when predicting O_2^- chemistry from modeled or observed photochemical H_2O_2 production.

4. CONCLUSIONS

Algorithms that derive *in situ* UV optical properties from remote sensing products are attractive in that they allow expanded spatial and temporal coverage when evaluating the role of photochemical reactions in the global ocean. To that end, we have expanded the methods of Fichot and Miller[26] for estimating photochemical rates from ocean color data to include MODIS SST data, and have presented what we feel is a more accurate calculation of H_2O_2 photoproduction rates in the surface ocean. By blending maps for UV optics and temperature, an improvement over the previous use of a single AQY spectrum for the entire global ocean has been achieved. In the case of H_2O_2, the known temperature dependence for peroxide photochemical efficiency, as defined with published activation energies,[19,23] can provide not only an improvement in estimated H_2O_2 photoproduction rates as shown here, but also a general approach for addressing any photochemical rate that has a definable temperature dependence. As is the case for all marine photochemical models using a photochemical efficiency approach, the accuracy with which peroxide production estimates can be made from optical data is primarily constrained by limited availability of H_2O_2 AQY spectral data and the ability to match observed variations in the surface ocean with proper AQY spectra. Improved confidence in this model to calculate global distributions of H_2O_2, O_2^-, or any other photochemical product, will require well-defined, improved knowledge of the mechanisms regulating the system of interest.

To push our model approach towards estimation of surface ocean H_2O_2 *concentrations*, additional H_2O_2 sources, like rain and biological production, together with both abiotic (i.e. chemical reactions and mixing) and biological H_2O_2 sinks must be accurately described and incorporated. On the source side, oceanic microwave-based

precipitation maps are available,[67,68] but the changing relation between rain rate and peroxide concentration over the ocean is not well constrained. Both production and consumption rates due to organisms depend on biological variability with additional sinks arising from chemical reactants (ex. Fe, Cu, organic antioxidants, etc.).[69,70] The detailed data required to modify and inform peroxide concentration models, especially in open ocean systems, are not currently fully retrievable from remote sensing and, the quantitative approaches to embed the temperature dependence for each are yet to be determined. With new comprehensive data on rates and mechanism, a concentration model for H_2O_2 in the surface ocean based on remotely sensed data may be attainable.

The method presented here to estimate O_2^- concentrations from H_2O_2 photoproduction rates is considerably more challenging than simply altering the H_2O_2 AQY spectra as a function of temperature. It actually represents a more general attempt to use remote sensing data together with direct knowledge of chemical reaction mechanisms to modify biogeochemical estimates related to photochemistry. We believe this is a promising direction for future work based on more than simple correlations. Our calculations rely heavily on the relationship between H_2O_2 and O_2^- photoproduction rates and the O_2^- decay kinetics in the open ocean. At present, much about the processes that control the fate of O_2^- are not completely understood. After new work quantifies the photo-efficiency for O_2^- production and better defines the magnitude and partitioning of various sinks for superoxide, our estimates of superoxide steady-state values will be much better constrained. Because pseudo-first order O_2^- decay is almost certainly affected by both temperature and pH (in the same way as biomolecular dismutation), new data on the effects of these variables on O_2^- decay reactions should put things a bit more

778 in focus. With this fundamental chemical information and clever use of multiple data
779 products generated from remotely sensed data (S, pH, mixed layer depth, precipitation,
780 etc.), it should be possible to quantify O_2^- concentrations with more accuracy on a global
781 scale under current and future oceanic conditions. Although well beyond the scope of the
782 present study, as more data on oceanic redox cycling becomes available, this approach
783 can be used to make reasonable global estimates for the lifetimes of various important
784 redox active elements like Fe, Cu and Mn, using their chemical reaction rates with ROS
785 in the surface ocean.
786
787 **Acknowledgements**
788 This work was supported by NSF grant OCE-1234388 and NASA grant
789 NNX07AD85G awarded to Dr. William L. Miller. The authors would like to thank
790 Lydia Babcock-Adams, Jade Enright and the captain and crew of *R/V Pelican* and *R/V*
791 *Melville* for sampling assistance and Dr. Wayne S. Gardner for the invitation to
792 participate on the *R/V Pelican* cruise, supported by NOAA-CSCOR grant number
793 NA07NOS4780225. We thank NASA for providing SeaWiFS, TOMS, and MODIS data
794 and the American Meteorological Society for graduate student support for L.C.P. to
795 attend the 2013 Duce Symposium at the 93rd AMS Annual Meeting, which led directly to
796 the development of this paper.
797
798
799
800

References

1 J. M. Burns, W. J. Cooper, J. L. Ferry, D. W. King, B. P. DiMento, K. McNeill, C. J. Miller, W. L. Miller, B. M. Peake, S. A. Rusak, A.L. Rose, T.D. Waite, Methods for Reactive Oxygen Species (ROS) Detection in Aqueous Environments, *Aquat. Sci*, 2012, **74**, 683-734.

2 D. J. Kieber, B. M. Peake, and N. M. Scully, Reactive Oxygen Species in Aquatic Ecosystems, in *UV Effects in Aquatic Organisms*, ed. E. V. Helbling and H. Zagarese, Royal Chemistry Society, Cambridge, UK, 2003, pp 251-288.

3 E. M. White, P. P. Vaughan and R. G. Zepp, Role of the Photo-Fenton Reaction in the Production of Hydroxyl Radicals and Photobleaching of Colored Dissolved Organic Matter in a Coastal River of the Southeastern United States, *Aquat. Sci.*, 2003, **65**, 402-414.

4 N. M. Scully, W. J. Cooper and L. J. Tranvik, Photochemical Effects on Microbial Activity in Natural Waters: the Interaction of Reactive Oxygen Species and Dissolved Organic Matter, *FEMS Microb. Ecol.*, 2003, **46**, 353-257.

5 Y. Chen, C. Hu, X. Hu and J Qu, Indirect Photodegradation of Amine Drugs in Aqueous Solution under Simulated Sunlight, *Environ. Sci. Technol.*, 2009, **43**, 2760-2765.

6 R. G. Zepp, T. V. Callaghan and D. J. Erickson III, Interactive Effects of Ozone Depletion and Climate Change on Biogeochemical Cycles, *Photochem. Photobiol. Sci.*, 2003, **2**, 51-61.

7 C. D. Clark, W. J. De Bruyn, S. D. Jakubowski and S. B. Grant, Hydrogen Peroxide Production in Marine Bathing Waters: Implications for Fecal Indicator Bacteria Mortality, *Mar. Pollut. Bull*., 2008, **56**, 397-401.

8 J. J. Morris, J. I. Johnson, M. J. Szul, M. Keller and E. R. Zinser, Dependence of the Cyanobacterium *Prochlorococcus* on Hydrogen Peroxide Scavenging Microbes for Growth at the Ocean's Surface, *PLoS ONE*, 2011, **6**(2), 1-13.

9 F. Baltar, T. Reinthaler, G. J. Herndl and J. Pinhassi, Major Effect of Hydrogen Peroxide on Bacterioplankton Metabolism in the Northeast Atlantic, *PLoS ONE*, 2013, **8**(4), 1-8.

10 J. W. Moffett and R. G. Zika, Reaction Kinetics of Hydrogen Peroxide with Copper and Iron in Seawater, *Environ. Sci. Technol.*, 1997, **21**, 804-810.

11 B. M. Voelker, and B. Sulzberger, Effects of Fulvic Acid on Fe(II) Oxidation by Hydrogen Peroxide, *Environ. Sci. Technol.*, 1996, **30**, 1106-1114.

12 A. L. Rose and T. D. Waite, Role of Superoxide in Photochemical Reduction of Iron in Seawater, *Geochim. Cosmochim. Acta*, 2006, **70**, 3869-3882.

13 K. Wuttig, M. I. Heller and P. L. Croot, Pathways of Superoxide (O_2^-) Decay in the Eastern Tropical North Atlantic, *Environ. Sci. Technol.*, 2013, **47**(18), 10249-10256.

14 Y. Zhang, R. Del Vecchio and N. V. Blough, Investigating the Mechanism of Hydrogen Peroxide Photoproduction by Humic Substances, *Environ. Sci. Technol.*, 2012, **46**(21), 11836-11844.

15 D. W. O'Sullivan, P. J. Neale, R. B. Coffin, T. J. Boyd and C. L. Osburn, Photochemical Production of Hydrogen Peroxide and Methylhydroperoxide in Coastal Waters, *Mar. Chem*, 2005, **97**(1-2), 14-33.

16 B. H. J. Bielski, D. E. Cabelli, R. L. Arudi and A. B. Ross, Reactivity of HO_2/O_2^- Radicals in Aqueous Solution, *J. Phys. Chem. Ref. Data.*, 1985, **14**(4), 1041-1100.

17 O. C. Zafiriou, Chemistry of Superoxide Ion-Radical (O_2^-) in Seawater. I. pK^*_{asw} (HOO) and Uncatalyzed Dismutation Kinetics Studied by Pulse Radiolysis*, *Mar. Chem.*, 1990, **30**, 31-43.

18 M. I. Heller and P. L. Croot, Superoxide Decay Kinetics in the Southern Ocean, *Environ. Sci. Technol.*, 2010, **44**, 191-196.

19 D. J. Kieber, G. W. Miller, K. Mopper and P. J. Neale, Wavelength and Temperature-Dependent Apparent Quantum Yields for Photochemical Formation of Hydrogen Peroxide in Seawater, *Environ. Sci.: Process. Impacts*, this issue.

20 S. S. Andrews, S. Caron and O. C. Zafiriou, Photochemical Oxygen Consumption in Marine Waters: A Major Sink for Colored Dissolved Organic Matter? *Limnol. Oceanogr.*, 2000, **45**(2), 267-277.

21 B. H. Yocis, D. J. Kieber and K. Mopper, Photochemical Production of Hydrogen Peroxide in Antarctic Waters, *Deep Sea Res. Part I: Oceanogr. Res. Papers,* 2000, **47**(6), 1077-1099.

22 R. Szymczak and T. D. Waite, Generation and Decay of Hydrogen Peroxide in Estuarine Waters. *Aust. J. Mar. Freshwater Res.*, 1988, **39**, 289-299.

23 G. W. Miller, Wavelength and Temperature-Dependent Apparent Quantum Yields for Photochemical Formation of Hydrogen Peroxide in Seawater, In *College of Environmental Science and Forestry*, State University of New York, Syracuse, NY, 2000.

24 M. I. Heller and P. L. Croot, Application of a Superoxide (O_2^-) Thermal Source (SOTS-1) for the Determination and Calibration of O_2^- Fluxes in Seawater, *Analytica Chimica Acta*, 2010, **667**, 1-13.

25 H. E. Reader and W. L. Miller, Variability of Carbon Monoxide and Carbon Dioxide Apparent Quantum Yield Spectra in Three Coastal Estuaries of the South Atlantic Bight, *Biogeosciences*, 2012, **9**, 4279-4294.

26 C. G. Fichot and W. L. Miller, An Approach to Quantify Depth-Resolved Marine Photochemical Fluxes Using Remote Sensing: Application to Carbon Monoxide (CO) Production, *Remote Sens. Environ.*, 2010, **144**(7), 1363-1377.

27 M. Ishii, M. Kimoto, K. Sakamoto and S. -I. Iwasaki, Steric Sea Level Changes Estimated from Historical Ocean Subsurface Temperature and Salinity Analysis, *J. Oceanogr.*, 2006, **62**, 155-170.

28 T. P. Boyer, S. Levitus, J. I. Antonov, R. A. Locarnini and H. E. Garcia, Linear Trends in Salinity for the World Ocean, *Geophys. Res. Lett.*, 2005, **32**, L01604.

29 M. Steinacher, F. Joos, T. L. Frölicher, G. -K. Plattner and S. C. Doney, Imminent Ocean Acidification in the Arctic Projected with the NCAR Global Coupled Carbon Cycle-Climate Model, *Biogeosciences*, 2009, **6**, 515-533.

30 S. C. Johannessen and W. L. Miller, Quantum Yield for the Photochemical Production of Dissolved Organic Carbon in the Ocean, *Mar. Chem.*, 2001, **76**, 271-283.
31 C. M. Swan, N. B. Nelson, D. A. Siegel and T. S. Kostadinov, The Effect of Surface Irradiance on the Absorption Spectrum of Chromophoric Dissolved Organic Matter in the Global Ocean, *Deep-Sea Res. I.*, 2012, **63**, 52-64.
32 D. W. King, W. J. Cooper, S. A. Rusak, B. M. Peake, J. J. Kiddle, D. W. O'Sullivan, M. L. Melamed, C. R. Morgan and S. M. Theberge, Flow Injection Analysis of H_2O_2 in Natural Water using Acridinium Ester Chemiluminescence: Method Development and Optimization using a Kinetic Model. *Anal. Chem.*, 2007, **79**, 4169-4179.
33 W. L. Miller and D. R. Kester, Hydrogen Peroxide Measurement in Seawater by (*p*-Hydroxyphenyl) Acetic Acid Dimerization, *Anal. Chem.*, 1988, **60**, 2711-2715.
34 A. L. Rose, J. W. Moffett and T. D. Waite, Determination of Superoxide in Seawater Using 2-Methyl-6-(4-methoxyphenyl)-3,7-dihydroimidazo[1,2-a]pyrazin-3(7*H*)-one Chemiluminescence, *Anal. Chem.*, 2008, **80**, 1215-1227.
35 S. Garg, A. L. Rose and T. D. Waite, Photochemical Production of Superoxide and Hydrogen Peroxide from Natural Organic Matter, *Geochim. Cosmochim. Acta*, 2011, **75**, 4310-4320.
36 K. Fujimori, H. Nakajima, K. Akutsu, M. Mitani, H. Sawada and M. Nakayama, Chemiluminescence of *Cypridina* Luciferin Analogues. Part 1. Effect of pH on Rates of Spontaneous Autoxidation of CLA in Aqueous Buffer Solutions, *J. Chem. Soc. Perkin Trans. 2*, 1993, **12**, 2405-2409.
37 K. Akutsu, H. Nakajima, T. Katoh, S. Kino and K. Fujimori, K, Chemiluminesce of *Cipridina* luciferin analogues. Part 2. Kinetic Studies on the Reaction of 2-Methyl-6-(4-methoxyphenyl)-3,7-dihydroimidazo[1,2-a]pyrazin-3(7*H*)-one (CLA) with Superoxide: Hydroperoxyl Radical is an Actual Active Species used to Initiate the Reaction. *J. Chem. Soc. Perkin Trans. 2*, 1995, **8**, 1699-1706.
38 M. S. McDowell, A. Bakač and J. H. Espenson, A Convenient Route to Superoxide Ion in Aqueous Solution. *Inorg. Chem.*, 1983, **22**, 847-848.
39 T. -C. Ong, Detailed Mechanistic and Optimization of the Photochemical Production Method of Superoxide, In *Department of Chemistry*, Colby College, Waterville, ME, 2007.
40 B. H. J. Bielski, Reevaluation of the Spectral and Kinetic Properties of $HO_2^{\cdot}$ And $O_2^{\cdot-}$ Free Radicals, *Photochem. Photobiol.*, 1978, **28**, 645-649.
41 S. P. Hansard, A. W. Vermilyea and B. M. Voelker, Measurements of Superoxide Radical Concentration and Decay Kinetics in the Gulf of Alaska, *Deep-Sea Res. I.*, 2010, **57**, 1111-1119.
42 J. V. Goldstone and B. M. Voelker, Chemistry of Superoxide Radical in Seawater: CDOM Associated Sink of Superoxide in Coastal Waters. *Environ. Sci. Technol.*, 2000, **34**(6), 1043-1048.
43 M. I. Heller and P. L. Croot, Kinetics of Superoxide Reactions with Dissolved Organic Matter in Tropical Atlantic Surface Waters near Cape Verde (TENATSO), *J. Geophys. Res.*, 2010, **115**, 1-13 (C12038).

44 M. I. Heller and P. L. Croot, Superoxide Decay as a Probe for Speciation Changes during Dust Dissolution in Tropical Atlantic Surface Waters near Cape Verde, *Mar. Chem.*, 2011, **126**, 37-55.

45 G. M. Marion, F. J. Millero, M.F. Camões, P. Spitzer, R. Feistel and C. -T. A. Chen, pH of Seawater, *Mar. Chem.*, 2011, **126**, 89-96.

46 E. J. D'Sa, R. G. Steward, A. Vodacek, N. V. Blough and D. Phinney, Determining Optical Absorption of Colored Dissolved Organic Matter in Seawater with a Liquid Capillary Waveguide, *Limnol. Oceanogr.*, 1999, **44**(4), 1142-1148.

47 H. E. Reader and W. L. Miller, Effect of Estimations of Ultraviolet Absorption Spectra of Chromophoric Dissolved Organic Matter on the Uncertainty of Photochemical Production Calculations*, J. Geophys. Res.,* 2011, **166**, C08002.

48 R. L. Miller, M. Belz, C. Del Castillo and C. Trzaska, Determining CDOM Absorption Spectra in Diverse Coastal Environments using a Multiple Pathlength, Liquid Core Waveguide System, *Continental Shelf Research*, 2002, **22**, 1301-1310.

49 N. B. Nelson, D. A. Siegel, C. A. Carlson, C. Swan, W. M. Smethie Jr and S. Khatiwala, Hydrography of Chromophoric Dissolved Organic Matter in the North Atlantic, *Deep Sea Res. I*, 2007, 710-731.

50 C. Hu, F. E. Muller-Karger and R. G. Zepp, Absorbance, Absorption Coefficient, and Apparent Quantum Yield: A Comment on Common Ambiguity in the Use of These Optical Concepts, *Limnol. Oceanogr.*, 2002, **47**(4), 1261-1267.

51 C. G. Fichot, S. Stahyendranath and W. L. Miller, Sea*UV* and SeaUV_c: Algorithms for the Retrieval of UV/Visible Diffuse Attenuation Coefficients from Ocean Color, *Remote Sens. Environ.*, 2008, **112**, 1584-1602.

52 R. Ruggaber, R. A. Dlugi and T. Nakajima, Modelling of Radiation Quantities and Photolysis Frequencies in the Troposphere. *J. Atmos. Chem.*, 1994, **18**, 171-210.

53 O. B. Brown and P. J. Minnett, MODIS Infrared Sea Surface Temperature Algorithm, Algorithm Theoretical Basis Document, Version 2.0, 1999, http://modis.gsfc.nasa.gov/data/atbd/atbd_mod25.pdf.

54 W. J. Cooper, R. G. Zika, R. G. Petasne and J. M. C. Plane, Photochemical Formation of H_2O_2 in Natural Waters Exposed to Sunlight. *Environ. Sci. Technol.*, 1988, **22**, 1156-1160.

55 C. A. Moore, C. T. Farmer and R. G. Zika, Influence of the Orinoco River on Hydrogen Peroxide Distribution and Production in the Eastern Caribbean, *J. Geophys. Res.*, 1993, **98**, 2289-2298.

56 R. M. Dalrymple, A. K. Carfagno and C. M. Sharpless, Correlations between Dissolved Organic Matter Optical Properties and Quantum Yields of Singlet Oxygen and Hydrogen Peroxide, *Environ. Sci. Technol.*, 2010, **44**, 5824-5829.

57 J. R. Helms, A. Stubbins, J. D. Ritchie, E. C. Minor, D. J. Kieber and K. Mopper, Absorption Spectral Slopes and Slope Ratios as Indicators of Molecular Weight, Source and Photobleaching of Chromophoric Dissolved Organic Matter, *Limnol. Oceanogr.*, 2008, **53**(3), 955-969.

58 S. Steigenberger and P. L. Croot, Identifying the Processes Controlling the Distribution H_2O_2 in Surface Waters Along a Meridional Transect in the Eastern Atlantic. *Geophys. Res. Lett.*, 2008, **35**, 1-5 (L03616).
59 E. Micinski, L. A. Ball and O. C. Zafiriou, Photochemical Oxygen Activation: Superoxide Radical Detection and Production Rates in the Eastern Caribbean, *J. Geophys. Res.*, 1993, **98**, 2299-2306.
60 A. L. Rose, E. A. Webb, T. D. Waite and J. W. Moffett, Measurement and Implications of Nonphotochemically Generated Superoxide in the Equitorial Pacific, *Environ. Sci. Technol.*, 2008, **42**, 2387-2393.
61 B. M. Voelker and D. L. Sedlak, Iron Reduction by Photoproduced Superoxide in Seawater, *Mar. Chem.*, 1995, **50**, 93-102.
62 Y. Shaked, R. Harris and N. Klein-Kedem, Hydrogen Peroxide Photocycling in the Gulf of Aqaba, Red Sea, *Environ. Sci. Technol.*, 2010, **44**, 3238-3244.
63 R. G. Petasne and R. G. Zika, Fate of Superoxide in Coastal Seawater, *Nature*, 1987, **325**, 516-518.
64 K. Wuttig, M. I. Heller and P. L. Croot, Reactivity of Inorganic Mn and Mn Desferrioxamine B with O_2, O_2^-, and H_2O_2 in Seawater, *Environ. Sci. Technol.*, 2013, **47**(18), 10257-10265.
65 A. Cudd and I. Fridovich, Electrostatic Interactions in the Reaction Mechanism of Bovine Erythrocyte Superoxide Dismutase, *J. Biol. Chem.*, 1982, **257**(19), 11443-11447.
66 S. A. Rusak, B. M. Peake, L. E. Richard, S. D. Nodder and W. J. Cooper, Distributions of Hydrogen Peroxide and Superoxide in Seawater east of New Zealand. *Mar. Chem.*, 2011, **127**, 155-159.
67 R. F. Alder, G. Gu and G. J. Huffman, Estimating Climatological Bias Errors for the Global Precipitation Climatology Project (GPCP), *J. Appl. Meteor. Climatol.*, 2012, **51**, 84–99. doi: http://dx.doi.org/10.1175/JAMC-D-11-052.1.
68 P. A. Kucera, E. E. Ebert, F. J. Turk, V. Levizzani, D. Kirschbaum, F. J. Tapiador, A. Loew and M. Borsche, Precipitation from Space: Advancing Earth System Science. *Bull. Amer. Meteor. Soc.*, 2013 **94**, 365–375, doi: http://dx.doi.org/10.1175/BAMS-D-11-00171.1.
69 K. M. Mostofa, C. Q. Liu, H. Sakugawa, D. Vione, D. Minakata and F. Wu, Photoinduced and Microbial Generation of Hydrogen Peroxide and Organic Peroxides in Natural Waters, in *Photobiogeochemistry of Organic Matter*, Spring, Berlin, Heidelberg, 2013, pp 139-207.
70 K. M. Mostofa, C. Q. Liu, K. Gao, S. Li, D. Vione and M. A. Mottaleb, Impacts of Global Warming on Biogeochemical Cycles in Natural Waters, in *Photobiogeochemistry of Organic Matter*, Spring, Berlin, Heidelberg, 2013, pp 851-915.

Figures and Tables

Table 1. Sample characteristics and $\varphi(\lambda)$ fitting parameters (m values with 95% confidence intervals) for laboratory H_2O_2 $\varphi(\lambda)$ determined at 20 °C for seawater samples from the Gulf of Mexico and the Gulf of Alaska (A). The r^2 is for the correlation between measured H_2O_2 production and that calculated from the $\varphi(\lambda)$ for all quartz cells in a given exposure. Sample characteristics and k_{pseudo} (s^{-1} with 95% confidence intervals) determined from non-linear curve fitting of shipboard superoxide decay curves (B).

(A)

Station	Latitude (N)	Longitude (W)	S (PSU)	$a_g(320)$ (m^{-1})	m_1	m_2	r^2
GoM1	28.97	89.11	26.5	2.82	7.23 ± 1.15	0.025 ± 0.017	0.91
GoM2	28.90	89.44	n.d.	6.64	6.88 ± 0.54	0.019 ± 0.007	0.98
GoM3	28.70	89.50	n.d.	3.57	8.87 ± 0.51	0.020 ± 0.008	0.98
GoM4	27.92	90.37	36.4	0.090	7.12 ± 1.41	0.025 ± 0.022	0.75
GoA1	53.00	152.00	34.5	0.279	8.23 ± 0.48	0.024 ± 0.011	0.96
GoA2	50.00	145.00	32.4	0.162	7.90 ± 1.02	0.027 ± 0.025	0.84
GoA Pooled	-	-	-	-	8.201 ± 0.47	0.0238 ± 0.011	0.92

(B)

Station	Latitude (N)	Longitude (W)	S (PSU)	$a_g(320)$ (m^{-1})	pH_{NBS}	k_{pseudo_3} (x 10^{-3} s^{-1})	r^2
GoA2	50.00	145.00	32.4	0.162	8.08	4.59 ± 0.08	0.96
GoA3	49.28	134.67	32.4	0.138	8.07	2.02 ± 0.03	0.91
GoA4	54.60	141.41	32.5	0.222	8.05	1.95 ± 0.02	0.94
GoA5	56.47	141.24	32.4	0.428	8.17	1.71 ± 0.04	0.89

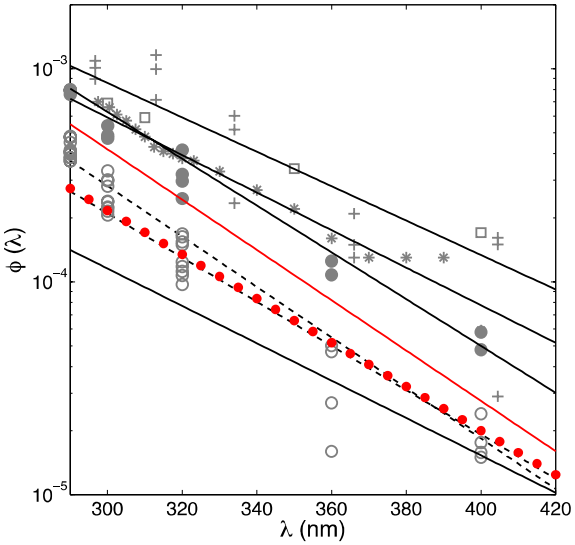

Figure 1. Apparent quantum yield spectra ($\varphi(\lambda)$) for H_2O_2 photoproduction at 20 °C for our Gulf of Mexico (solid line) and the Gulf of Alaska (dashed line) experiments (this study). The red dotted line is the pooled AQY spectrum for both Gulf of Alaska stations. Select AQY data from other studies are also shown: Kieber et al.[19] average seawater AQY spectrum adjusted to 20 °C (solid red line), Miller[23] Antarctic at 15 °C (open circle), Miller[23] Station ALOHA at 15 °C (closed circle), Cooper et al.[54] VH Pond, Florida (*), Moore et al.[55] Orinoco River outflow (+) and Andrews et al.[20] 1:5 Shark River water (open squares).

Table 2. Average, maximum and minimum H_2O_2 production rates (nM d^{-1}) for the global ocean at 1 m depth for each month.

	Jan	Feb	Mar	Apr	May	Jun	Jul	Aug	Sep	Oct	Nov	Dec
Avg	48.7	47.1	44.6	42.3	43.2	42.9	42.4	41.6	43.5	46.6	48.3	48.5
Max	96.0	92.3	93.9	93.2	99.6	102.1	105.6	100.6	100.6	97.1	98.8	99.2
Min	0.06	0.06	0.06	0.12	0.05	0.09	0.11	0	0.06	0.05	0.03	0.08

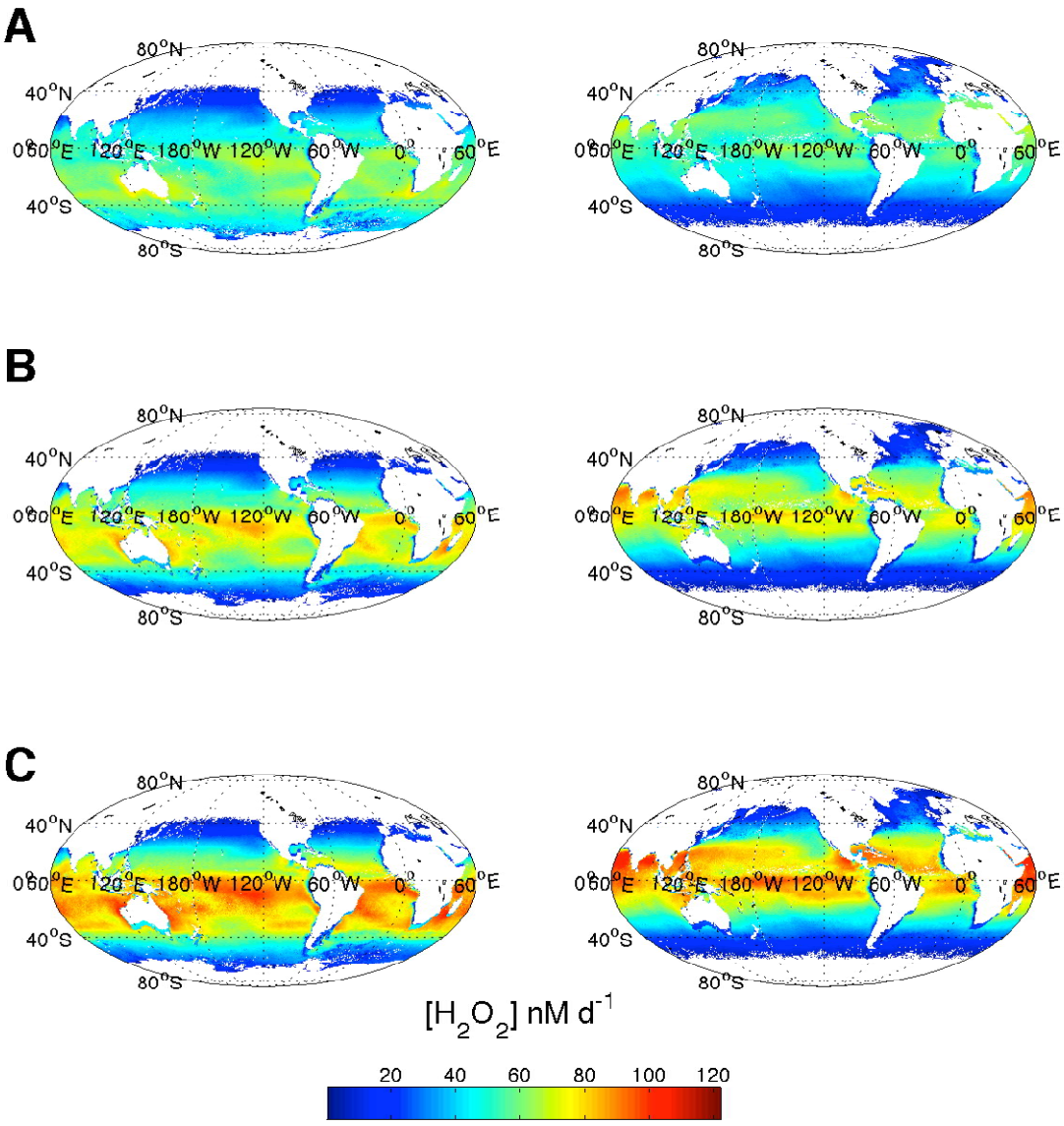

Figure 2. H_2O_2 photoproduction rates (nM d^{-1}) at 1 m depth for January (left) and April (right). Areas in white are where SeaWiFS ocean color is not available. 3 different quantum yields for H_2O_2 were used to create these climatologies: **(A)** The single pooled AQY spectrum not modified for temperature variation, **(B)** the AQY spectrum adjusted for temperature using current MODIS SST climatologies and **(C)** the AQY spectrum was adjusted for temperature with SST 5 °C higher than current MODIS climatologies.

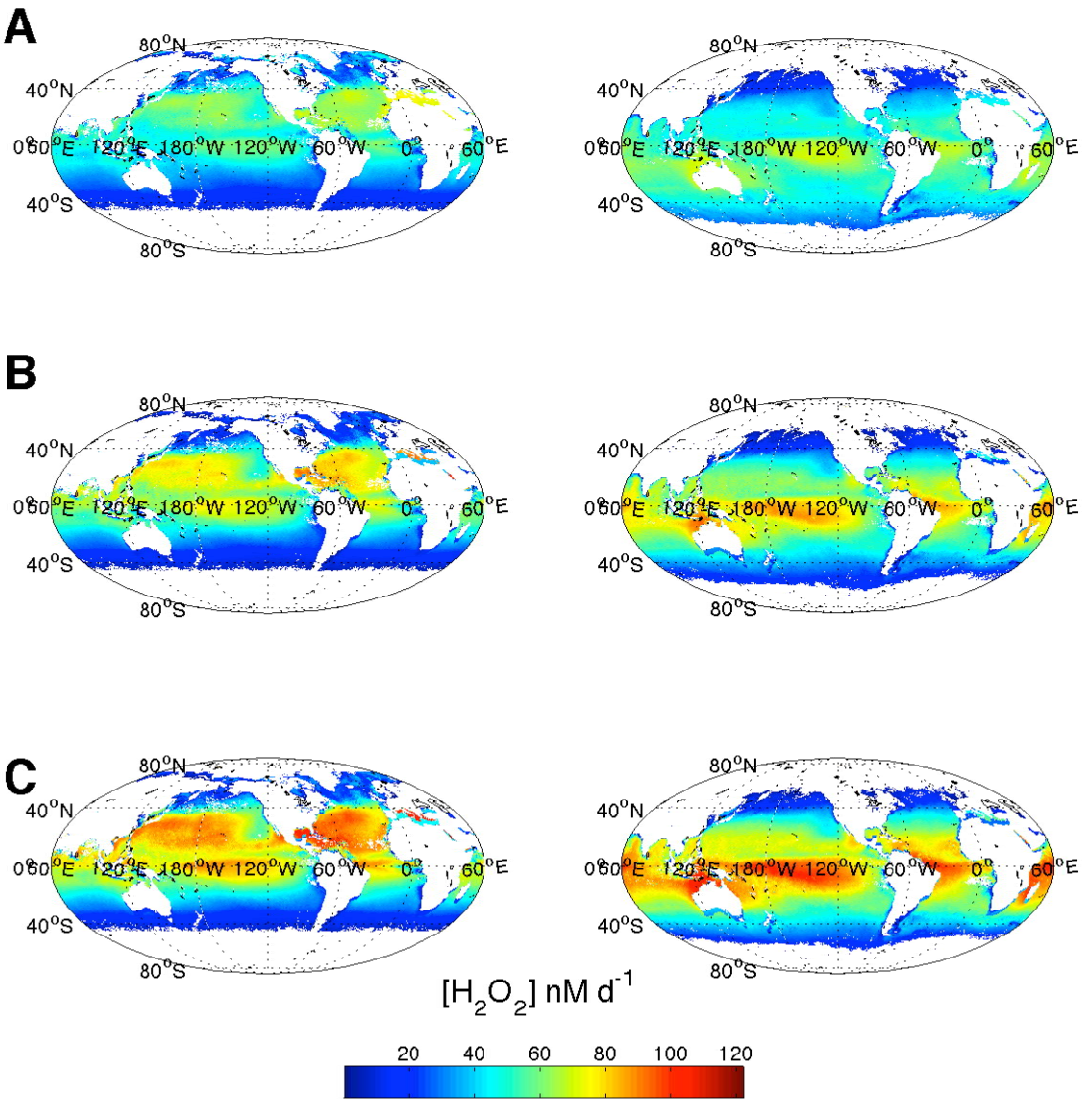

Figure 2 (continued). H_2O_2 photoproduction rates (nM d^{-1}) at 1 m depth for July (left) and October (right). All other as presented above.

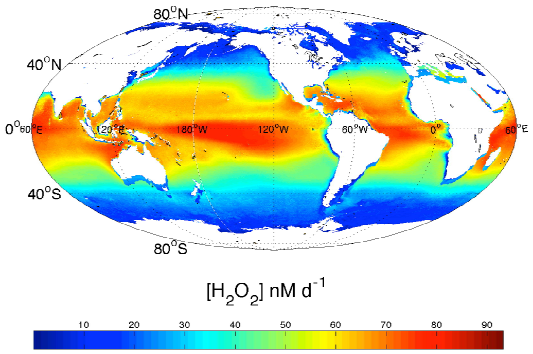

Figure 3. H_2O_2 photoproduction rates (nM d^{-1}) at 1 m for the entire year, calculated by averaging monthly climatologies created using temperature-modified AQY spectra. Areas in white are where SeaWiFS ocean color is not available.

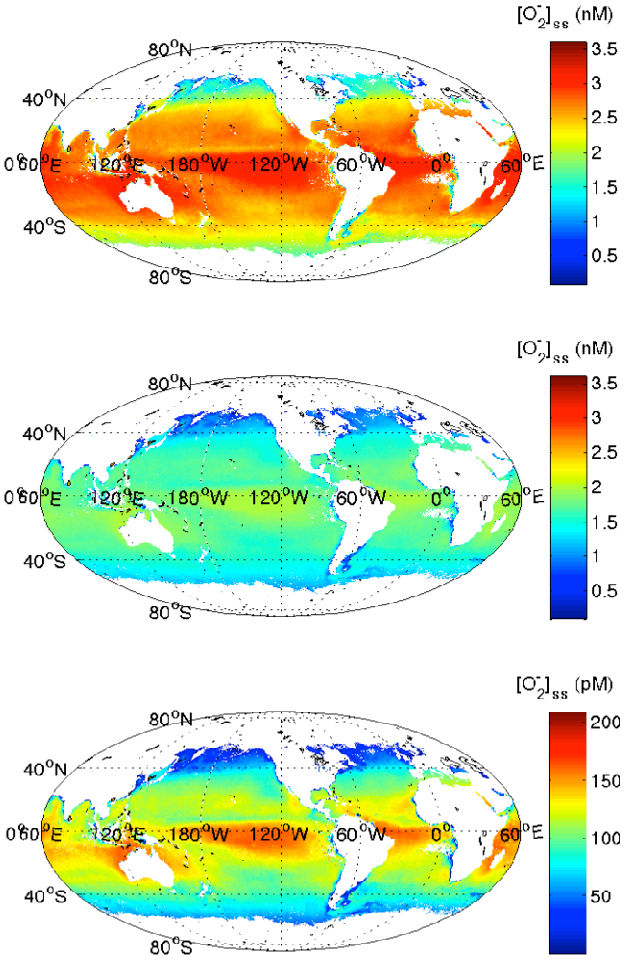

Figure 4. $[O_2^-]_{ss}$ (nM or pM) determined at 1 m for October: (Top) with O_2^- assumed to decay solely through dismutation at pH = 8.2, (Middle) with O_2^- assumed to decay solely through dismutation at pH = 7.8, (Bottom) with additional sinks added to dismutation at pH = 8.2 in order to more completely describe O_2^- decay.

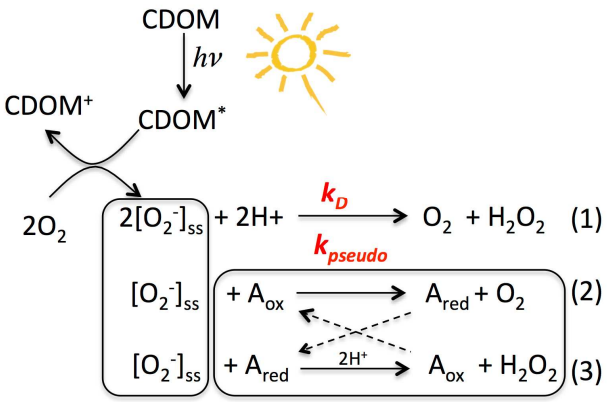

Figure 5. Possible mechanistic pathways for H_2O_2 production by O_2^-. A_{ox} and A_{red} are oxidized and reduced forms respectively of an unidentified reactant, A. Dashed lines represent the possible catalytic cycling of a single redox catalyst participating in both the oxidation and reduction of O_2^-.

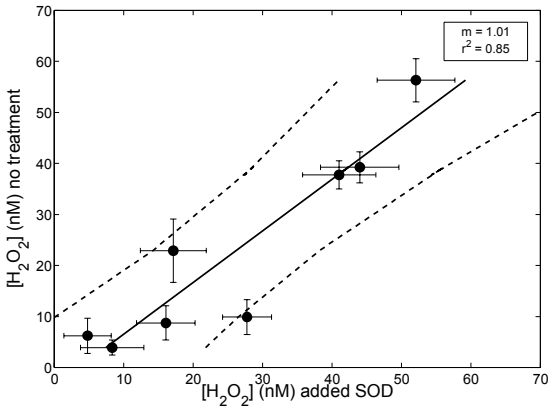

Figure 6. $[H_2O_2]$ (nM) produced during short (<3 h) irradiations of low CDOM seawater plotted against $[H_2O_2]$ produced in the presence of 200 U L^{-1} SOD. The solid line represents the linear regression between $[H_2O_2]$ produced during both treatments (m = 1.01, r^2 = 0.85) and the dashed lines are the 95% confidence interval.